ARCHIVES OF ELECTRICAL ENGINEERING VOL. 72(4), pp. 971–986 (2023)

DOI 10.24425/aee.2023.147421

Frequency control of voltage sourced converter-based multi-terminal direct current interconnected system based on virtual synchronous generator

CONGSHAN LI ✉, XIAOWEI ZHANG, PING HE, ZIKAI ZHEN, KEFENG ZHAO

College of Electrical Information Engineering, Zhengzhou University of Light Industry China

e-mail: {✉543627767/1458696052/865116082/736987041}@qq.com, hplkz@126.com

(Received: 02.04.2023, revised: 16.08.2023)

Abstract: In response to the inability of the flexible DC transmission system connected to the AC grid under conventional control strategies to provide inertia to the system as well as to participate in frequency regulation, a virtual synchronous generator (VSG) control strategy is proposed for a voltage source converter (VSC)-based multi-terminal high-voltage direct current (VSC-MTDC) interconnection system. First, the virtual controller module is designed by coupling AC frequency and active power through virtual inertia control, so that the VSC-MTDC system can provide inertia response for AC grid frequency. Second, by introducing the power margin of the converter station into the droop coefficient, the unbalanced power on the DC side is reasonably allocated to reduce the overshoot of the DC voltage in the regulation process. Finally, the power regulation capability of the normal AC system is used to provide power support to the fault end system, reducing frequency deviations and enabling inter-regional resource complementation. The simulation model of the three-terminal flexible DC grid is built in PSCAD/EMTDC, and the effectiveness of the proposed control strategy is verified by comparing the conventional control strategy and the additional frequency control strategy.

Key words: adaptive droop control, power margin, VSG, VSC-MTDC

1. Introduction

With the rapid development of renewable energy, large-scale wind farms are connected to the existing power grid through the voltage source converter-based multi-terminal direct current (VSC-MTDC) system [1–3]. However, since the grid-connected inverter has no rotational inertia,

the power grid is prone to frequency deviation when disturbed by disturbances [4]. Since the VSC-MTDC system can realize the independent control of active and reactive power, and the operation mode is flexible, appropriate control strategies can be designed to make the VSC-MTDC system provide inertial support to the AC system and participate in the AC frequency regulation.

Droop control can achieve power regulation through multiple VSC-stations to improve DC voltage stability, therefore, it has been widely used in the VSC-MTDC system [5–7]. The conventional droop control strategy focuses only on controlling the voltage stability of the DC network and the power distribution between the VSC stations, and cannot automatically adapt to the operating status of the AC network [8, 9].

To enable the VSC-MTDC system to participate in frequency control on the AC side, many solutions have been proposed in the literature. In [10, 11], it was proposed to superimpose the frequency outer-loop output on the droop control power reference of the VSC-station to enable the VSC-station to respond to AC system frequency variations. However, the real-time operating state of the DC system is not taken into account. In [12], it was proposed to use the rotor kinetic energy of wind turbines to participate in frequency control. However, extracting too much kinetic energy from the rotor can cause the turbine to stall, and restoring the rotor speed is a difficult task.

In recent years, virtual synchronous generator (VSG) technology has attracted considerable attention from researchers. This technology can be used by power electronic converters to make them have characteristics such as inertia and damping of the synchronous generator (SG), which simulate the process of active frequency regulation and reactive voltage regulation of synchronous machines from external characteristics, and thus improving the stability of AC systems [13–15]. In [16], it was proposed to embed the VSG core algorithm into the upper controller of the converter, simulate the SG active frequency modulation characteristics of the VSG, and adaptively adjust the droop coefficient through the frequency deviation margin. However, this may affect the stability of the DC voltage.

In [17], the virtual governor module is further designed based on VSG technology, small signal modelling of VSG control is performed, and controller parameter tuning is developed. In [18], the VSG technique with active fuzzy PI droop control was introduced into the VSC-MTDC system. By adjusting the droop coefficient, the converter is able to balance the AC frequency and DC voltage. In [19], the influence of inertia coefficient and damping coefficient on the performance of the controller is analyzed by the phase plane method, and the influence of virtual impedance on the transient stability of the system is also considered. When the VSG control is used to participate in the AC-side frequency regulation, the design of appropriate control strategies to reduce the DC voltage distortion is a problem worthy of in-depth study.

In this paper, the virtual inertia technique is applied to a VSC-MTDC interconnected system consisting of several AC grids. First, the active power on the DC side is coupled to the frequency on the AC side, and an expression for the coefficient between the active power on the DC side and the system frequency on the AC side is derived. Second, the power margin of the converter station is introduced into the droop coefficient to reasonably distribute the unbalanced power on the DC side and reduce the DC voltage deviation. Finally, the power support capability of the interconnected AC system is used to achieve inter-regional resource complementarity. Simulation results show that the proposed control strategy can effectively reduce the frequency deviation of the incident end system and improve the inertia support capability and primary frequency modulation capability of the interconnected system.

2. VSG control feasibility analysis

2.1. VSG control principle

Conventional power system inertia is provided by the energy stored in the rotor of the synchronous generator, which stores energy E_s as

$$E_s = \frac{1}{2} J \omega_0^2 , \tag{1}$$

where: J is the rotational inertia of the synchronous generator; ω_0 is the rated rotor speed.

The energy stored in the DC capacitor E_c is

$$E_c = \frac{1}{2} C_0 U^2 , \tag{2}$$

where: U is the DC capacitance voltage; C_0 is the DC capacitance value.

Comparing (1) and (2), the energy of the converter capacitor in the VSC-MTDC system can be considered to provide inertia to the system by simulating the characteristics of synchronous generator. As shown in Fig. 1.

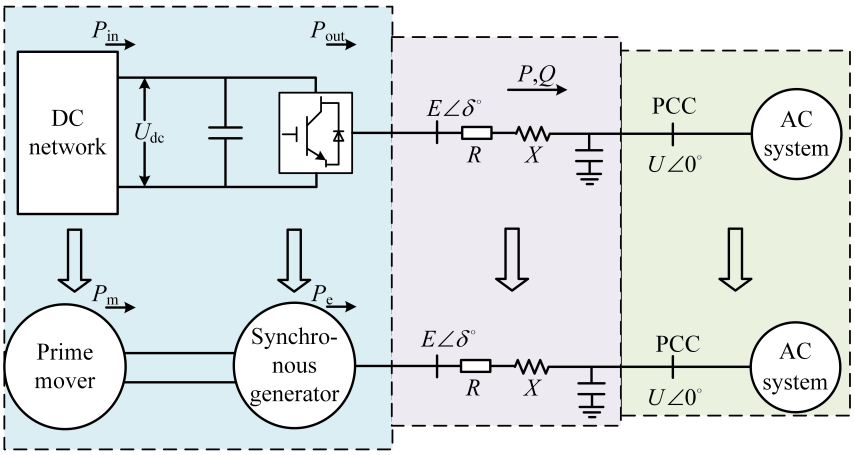

Fig. 1. Comparison of VSG machine and synchronous generator

In Fig. 1, the inverter potential e is equivalent to the internal potential of the synchronous generator; the reactance X is equivalent to the armature reactance of the synchronous generator; R is equivalent to the armature resistance. The mechanical power of the VSC is provided by the DC side; taking PCC as the reference point, if the voltage on the PCC bus is $U\angle 0°$, then the voltage at the AC side bus of the VSC is $E\angle\delta°$; the mechanical power output of the prime mover is P_m, and its output electromagnetic power is P_e.

In the AC system, the power balance of a synchronous generator can be expressed by the classical rotor equation of motion

$$2H\frac{\mathrm{d}\omega}{\mathrm{d}t} = P_m - P_e = \Delta P_1 , \tag{3}$$

where: H is the generator inertia time constant, ω is the actual angular velocity [20].

In the DC system, the DC side capacitance voltage power equation of the VSC-station is

$$\frac{N_{\mathrm{m}} C U_{\mathrm{dc}}}{S_{\mathrm{vsc}}} \frac{\mathrm{d}U_{\mathrm{dc}}}{\mathrm{d}t} = P_{\mathrm{in}} - P_{\mathrm{out}} = \Delta P_2 \,, \tag{4}$$

where: N_{m} is the number of DC capacitors; C is the capacitance value of the parallel connection in the VSC-station; S_{vsc} is the rated capacity of a single VSC station. U_{dc} is the measured DC voltage; P_{in} and P_{out} are the input and output power of the converter, respectively [21].

2.2. VSG control strategy considering the virtual governor

According to (3), if the generator's mechanical power and the electromagnetic power of the generator are not balanced, the rotor speed will change and the kinetic energy of the rotor will compensate for part of the power deficit, while the governor will adjust the power input to the prime mover according to the rotor speed. According to (4), if there is an unbalance in the DC system, the capacitor on the DC side of the inverter will charge and discharge until the system reaches a new state of equilibrium. Therefore, based on the above similar relationship, this paper considers the DC network as the prime mover and the converter as the synchronous generator, and designs the VSG control strategy considering the virtual governor. The additional power setpoint generated by the VSG control strategy consists of two components

$$\Delta P_{\mathrm{vsc}} = \Delta P_{\mathrm{vsg}} + \Delta P_{\mathrm{vg}} \,, \tag{5}$$

where: ΔP_{vsc} is the total additional power; ΔP_{vsg} is the additional power generated by the VSG; ΔP_{vg} is the additional power generated by the virtual governor.

ΔP_{vsg} can be obtained by simulating the rotor equation of a synchronous generator, whose expression is

$$\Delta P_{\mathrm{vsg}} = J \frac{\mathrm{d}\omega}{\mathrm{d}t} + D(\omega - \omega_{\mathrm{ref}}), \tag{6}$$

where: D is the damping coefficient; ω_{ref} is the rated angular frequency.

To obtain the additional power command ΔP_{vg} for the virtual governor, make the left sides of (3) and (4) equal

$$2H_{\mathrm{vsc}} \frac{\mathrm{d}\omega}{\mathrm{d}t} = \frac{N_{\mathrm{m}} C U_{\mathrm{dc}}}{S_{\mathrm{vsc}}} \frac{\mathrm{d}U_{\mathrm{dc}}}{\mathrm{d}t} \,, \tag{7}$$

where H_{vsc} represents the virtual inertia constant.

The indefinite integration of the two ends of (7)

$$2H_{\mathrm{vsc}}\omega = \frac{N_{\mathrm{m}} C U_{\mathrm{dc}}^2}{2S_{\mathrm{vsc}}} + m, \tag{8}$$

where m is the integration constant calculated from the rated angular frequency of ω_{ref} and the reference value of the DC voltage $U_{\mathrm{dc\,ref}}$ [22].

$$m = 2H_{\mathrm{vsc}}\omega_{\mathrm{ref}} - \frac{N_{\mathrm{m}} C U_{\mathrm{dc\,ref}}^2}{2S_{\mathrm{vsc}}} \,. \tag{9}$$

Substituting (9) into (8), performing a Taylor expansion and ignoring the higher terms, we get

$$U_{\mathrm{dc}} - U_{\mathrm{dc\,ref}} = \frac{4H_{\mathrm{vsc}}S_{\mathrm{vsc}}(\omega - \omega_{\mathrm{ref}})}{N_{\mathrm{m}}C(U_{\mathrm{dc}} + U_{\mathrm{dc\,ref}})}\,. \tag{10}$$

According to the calculation of the synchronous generator inertia time constant, the expression of the virtual inertia constant is

$$H_{\mathrm{vsc}} = \frac{N_{\mathrm{m}}CU^2}{2S_{\mathrm{vsc}}}\,. \tag{11}$$

The relationship between DC voltage and active power in the droop control of the VSC-station is

$$U_{\mathrm{dc}} = U_{\mathrm{dc\,ref}} + k\,(P_{\mathrm{s}} - P_{\mathrm{s\,ref}})\,, \tag{12}$$

where: k is the DC voltage droop coefficient, P_{s} and $P_{\mathrm{s\,ref}}$ are the actual and reference values of the active power of the VSC-station, respectively [23].

The coupling relationship between active power and frequency can be obtained from (10) and (12)

$$P_{\mathrm{s}} = P_{\mathrm{s\,ref}} + \frac{4H_{\mathrm{vsc}}S_{\mathrm{vsc}}}{N_{\mathrm{m}}Ck(U_{\mathrm{dc}} + U_{\mathrm{dc\,ref}})}(\omega - \omega_{\mathrm{ref}}). \tag{13}$$

Then, the expression for the active power-frequency droop coefficient k_{m} is

$$k_{\mathrm{m}} = \frac{4H_{\mathrm{vsc}}S_{\mathrm{vsc}}}{N_{\mathrm{m}}Ck(U_{\mathrm{dc}} + U_{\mathrm{dc\,ref}})}\,. \tag{14}$$

Furthermore, the additional power ΔP_{vg} can be written as

$$\Delta P_{\mathrm{vg}} = k_{\mathrm{m}}(\omega - \omega_{\mathrm{ref}}). \tag{15}$$

According to (15), the virtual governor can automatically adjust the active power of the VSC-station according to the frequency deviation. The governor control principle is shown in Fig. 2.

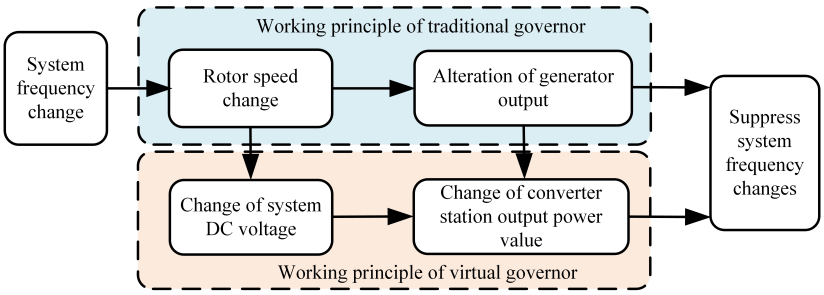

Fig. 2. Working principle of the virtual governor

In summary, the value of the power generated by the VSG can be expressed as

$$\Delta P_{\mathrm{vsc}} = J\frac{\mathrm{d}\omega}{\mathrm{d}t} + D(\omega - \omega_{\mathrm{ref}}) + \frac{4H_{\mathrm{vsc}}S_{\mathrm{vsc}}(\omega - \omega_{\mathrm{ref}})}{N_{\mathrm{m}}Ck(U_{\mathrm{dc}} + U_{\mathrm{dc\,ref}})}\,. \tag{16}$$

As can be seen from (16), the damping coefficient D and the active power-frequency droop coefficient k_m, although possessing different physical meanings, are both ratios of power deviation to frequency deviation and are in the same position in the control [24]. However, the damping coefficient equivalently increases the active power-frequency droop coefficient k_m, while making the power distribution of the converter no longer proportional to the droop coefficient, reducing the accuracy of the power distribution between VSC-stations.

The control block diagram of the VSC-MTDC system based on VSG control is given in Fig. 3.

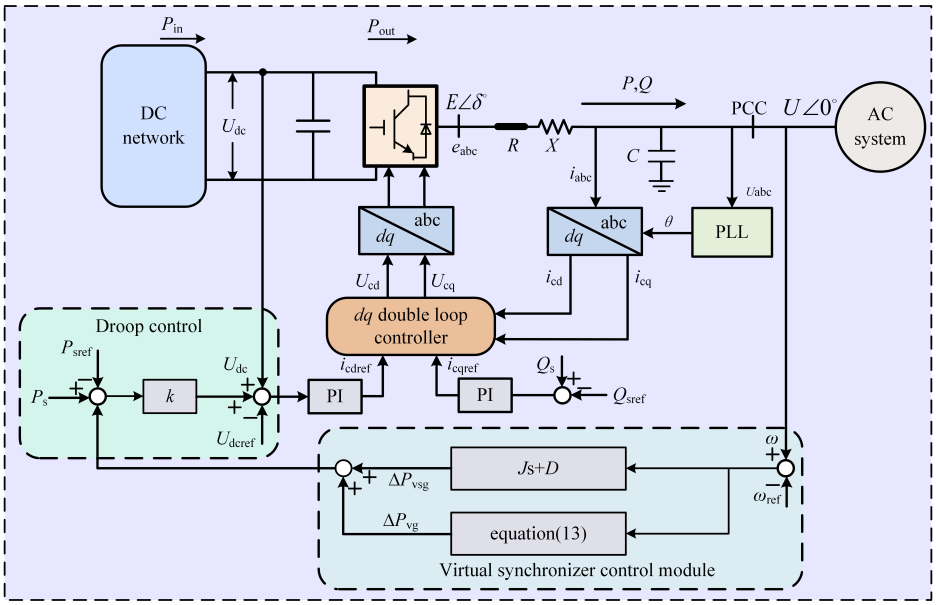

Fig. 3. Block diagram of VSC-MTDC control based on VSG control

3. Adaptive droop control strategy considering power margin

3.1. Conventional droop control

The structure of the conventional droop controller is shown in Fig. 4.

In Fig. 4, K_p and K_i are the PI control parameters of the VSC active power outer loop, respectively. $i_{cd\,ref}$ is the current reference value on the d-axis.

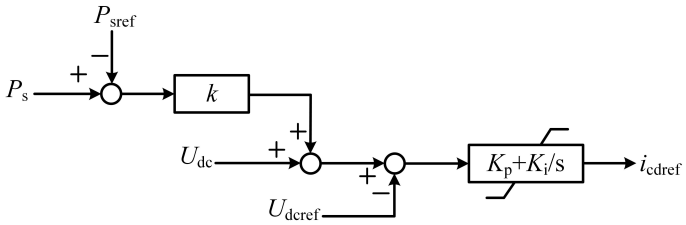

Fig. 4. Conventional droop controller

In the DC system, suppose there are N VSC-stations using the voltage droop control strategy. When power disturbance ΔP occurs in the DC system, each droop station automatically finds a new balance point through the droop curve. When the system reaches a new stable state with a change in the DC voltage of ΔU_{dc}, the relationship between the unbalanced power ΔP_i and the DC voltage ΔU_{dc} borne by the VSC$_i$-station ($0 < i < N$) is as follows:

$$\Delta P_i = \frac{\Delta U_{\mathrm{dc}}}{k_i}, \tag{17}$$

where k_i is the droop coefficient of the i-th VSC-station.

The total power disturbance value of the system ΔP should be equal the sum of the unbalanced power carried by the N droop stations for the whole DC system.

$$\Delta P = \sum_{i=1}^{N} \Delta P_i = \Delta U_{\mathrm{dc}} \sum_{i=1}^{N} \frac{1}{k_i}. \tag{18}$$

Combining (17) and (18)

$$\Delta P_i = \frac{\Delta P}{k_i \sum_{i=1}^{N} \frac{1}{k_i}}. \tag{19}$$

Equation (19) shows that the unbalanced power carried by the VSC-station is inversely proportional to its droop coefficient when the droop coefficient is fixed. Usually, each VSC-station's droop coefficient, which is typically inversely correlated to its VSC-station rated capacity, ensures that the VSC-station with the higher rated capacity bears more unbalanced power [25].

3.2. ADC Strategy

The principle of ADC is as follows: for VSC-stations with DC voltage droop control, the initial droop coefficient is first determined according to the principle of inverse proportion to the rated capacity, and then automatically corrected according to the power margin available in the VSC-station [26]. According to the above principle, the droop coefficient can be defined as

$$k_i = \begin{cases} \left(0.5 + \dfrac{P_{\mathrm{s\,max}} + P_{\mathrm{s}}}{2P_{\mathrm{s\,max}}}\right)^{\eta} \times k & P_{\mathrm{s}} > 0 \\ \left(0.5 + \dfrac{P_{\mathrm{s\,max}} - P_{\mathrm{s}}}{2P_{\mathrm{s\,max}}}\right)^{\eta} \times k & P_{\mathrm{s}} \le 0 \end{cases}, \tag{20}$$

where: $P_{\mathrm{s\,max}}$ is the VSC-station's rated capacity. η is defined as the power impact coefficient. Considering the different values of the initial active power command of the VSC-station, too large a value of η may lead to an over-correction of the droop coefficient and weaken the ability of the VSC-station to regulate the unbalanced power; too small value of η may cause full load regulation problems in the VSC-station.

By substituting the parameters into (20), the relationship between droop coefficient k_i and active power P_{s} and η can be obtained. As can be seen from Fig. 5, as the power margin increases, and the unbalanced power borne by the VSC-station during dynamic regulation is equivalent to increase.

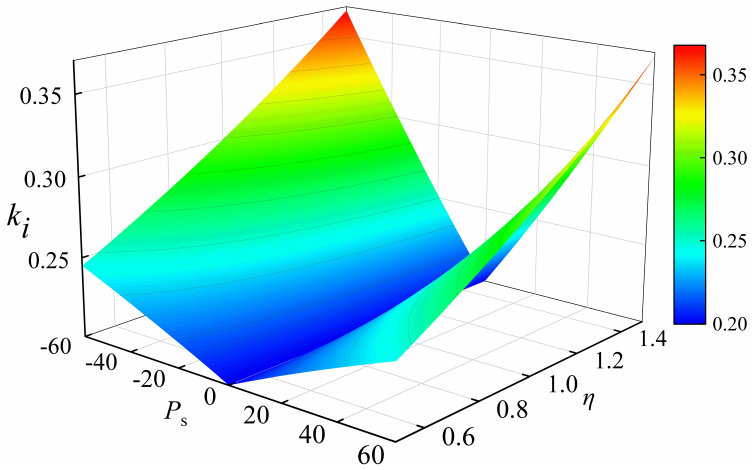

Fig. 5. Characteristic graph of adaptive droop coefficient

3.3. Comparison with the variable droop coefficients

This section aims to give the comparison in theoretical analysis with the available droop control schemes to demonstrate the improved performances under the proposed strategy.

In the variable droop coefficient scheme, the droop coefficient is calculated as [27]

$$k_i = k\,(1 + \alpha\Delta f)\left(1 + \beta\frac{\Delta P}{P_{\mathrm{s\,max}} - P_{\mathrm{s\,ref}}}\right), \tag{21}$$

where: α is the frequency deviation coefficient; β is the power margin coefficient.

From (20) and (21), it can be seen that both control strategies take into account the power margin of the VSC-station, a smaller droop coefficient is assigned to the converter with a larger power margin to take larger portion of the power distribution.

The difference between (20) and (21) lies in the relationship between the power margin and the droop coefficient. Equation (20) establishes the relationship between the real-time power margin and the droop coefficient, which can better adjust the droop coefficient adaptively according to the real-time operating status of the VSC-station and gives the value range of η.

Equation (21) introduces the frequency deviation and power deviation, and corrects the droop coefficient in the dynamic adjustment process through two variable parameters. However, there is still a fixed power margin in (21), which makes it difficult to accurately control the power distribution proportion of the VSC-station.

4. Simulation and analysis

4.1. Introduction to the simulation model

Based on the PSCAD/EMTDC simulation platform, a three-terminal VSC-MTDC system model is built as shown in Fig. 6. AC1~AC3 are active AC systems; VSC1 and VSC2 are rectifier

stations, and VSC3 is the inverter station. Figure 7 shows the adjustment part of the control circuit in the PSCAD. Table 1 shows the simulation parameters of the system. The control methods used in the comparison experiments are as follows:

CM1: $P - U$ conventional droop control,

CM2: Variable droop coefficient in [27],

CM3: The control strategy proposed in this paper.

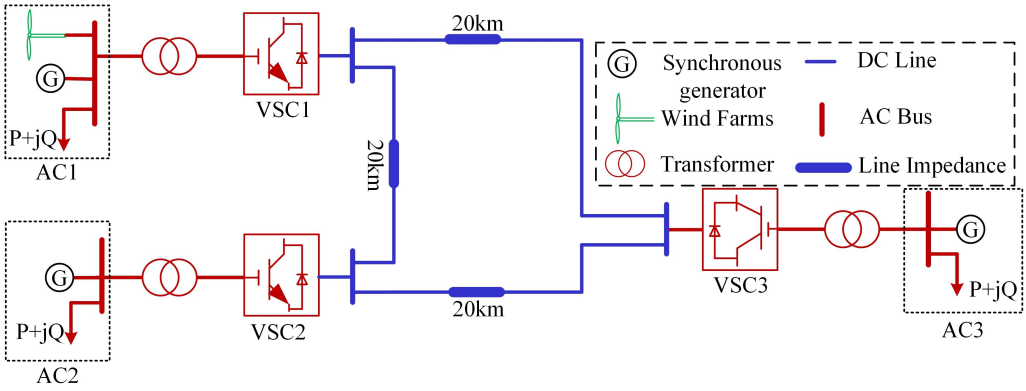

Fig. 6. Model of three-terminal VSC-MTDC system

Table 1. System simulation parameters

Parameter name	Symbol	Value	Unit
Rated capacity VSC1/VSC2/VSC3	S_{vsc}	60/60/120	MW
Nominal DC voltage	$U_{\text{dc ref}}$	200	kV
Nominal AC voltage	U_{ac}	110	kV
Capacitor number in each VSC	N_{m}	2	/
DC capacitor	C	1500	μF
Transformer ratio	/	110/100	/
DC line unit impedance	/	0.01	Ω/km
Rated frequency	f_{ref}	50	Hz
AC1/AC2/AC3 installed capacity	/	384/288/288	MW
Wind power	/	100	MW
Initial droop coefficient	k1/k2/k3	0.2/0.2/0.1	/
Rotational inertia	J	5.5	kg·m^2
Damping coefficient	D	1	N·m·s·rad^{-1}

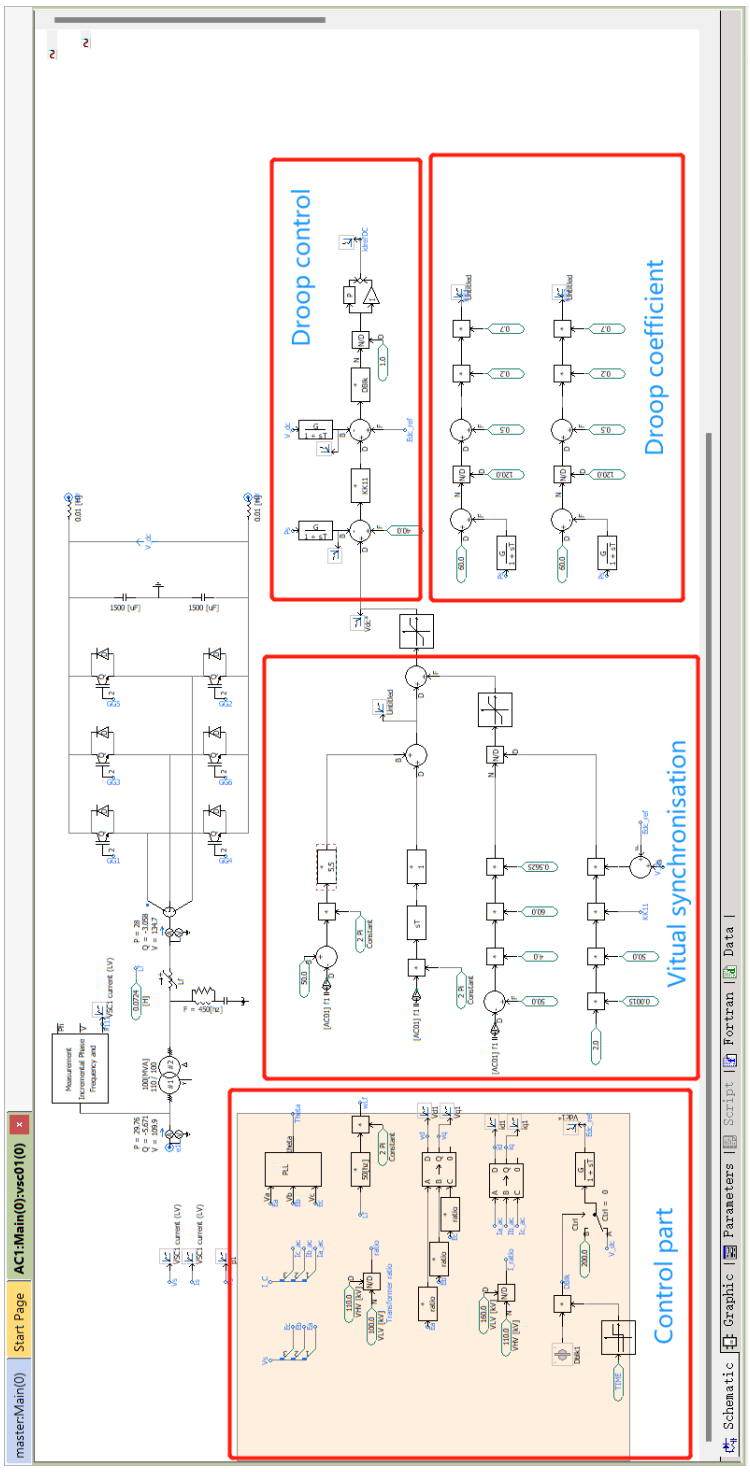

Fig. 7. Simulation circuit in PSCAD

4.2. Sudden increase of power grid load at the receiving end system

Load fluctuation is the most common fault in power systems. At t = 5 s, AC3 load increases by 20 MW, and the simulation results of CM1, CM2 and CM3 are shown in Fig. 8.

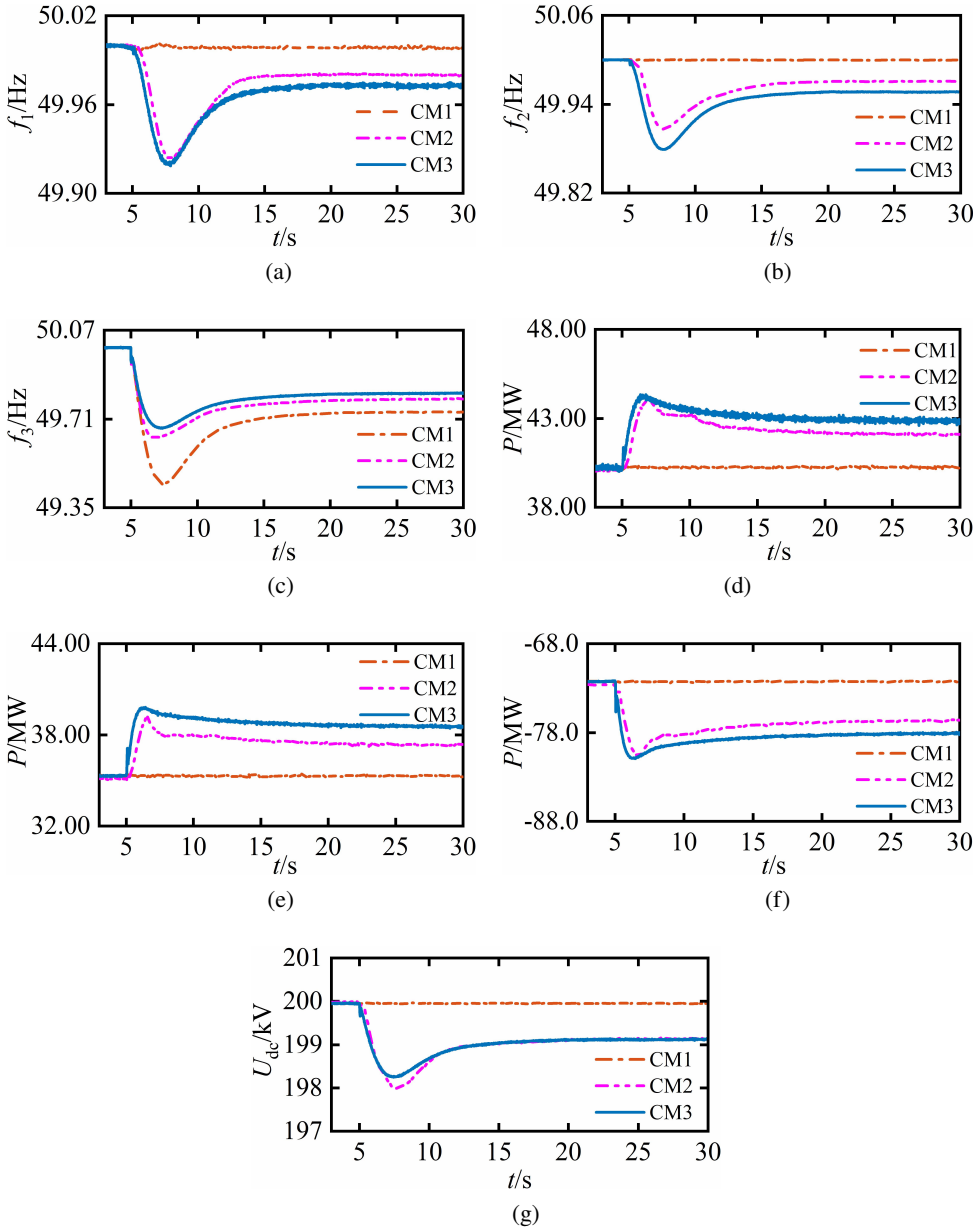

Fig. 8. AC3 active load increase simulation: AC1 frequency (a); AC2 frequency (b); AC3 frequency (c); VSC1 active power (d); VSC2 active power (e); VSC3 active power (f); system DC voltage (g)

Let $f_1 - f_3$ and $\Delta f_1 - \Delta f_3$ be the frequencies of AC1–AC3 and their variations, respectively, and $P_1 - P_3$ and $\Delta P_1 - \Delta P_3$ be the active power transmitted by VSC1–VSC3 and their variations, respectively. As shown in Fig. 8(c), under the control of CM1, f_3 drops to 49.45 Hz, $f_1 - f_2$ remain unchanged at 50 Hz, and the value of active power transmitted by the three VSC-stations remains unchanged. This is because the VSC-MTDC system can isolate faults on the AC side, and AC3 can only achieve active balancing through the frequency regulation performance of the generator set itself and the operating frequency characteristics of the load, resulting in large fluctuations in f_3. Under the control of CM2, the remaining VSC-stations provide power boost to the faulty AC system according to the DC voltage changes to the faulty AC system for power support. When the system reaches a stable state, $\Delta f_1 - \Delta f_3$ are 0.02, 0.03 and 0.21 Hz, $\Delta P_1 - \Delta P_3$ are 2.03, 2.22 and 3.96 MW, respectively. Although AC3 has greatly improved the frequency drop after obtaining power support from the remaining VSC-stations, and the droop coefficient has been reasonably adjusted according to the power margin of each VSC-station to improve the stable operation of the weak AC system. However, AC1 and AC2 have not fully utilized their frequency regulation capabilities to support the failed system at a fixed power margin.

Under the control strategy of this paper, the frequency regulation capability of the normal AC system is further released to support the fault-side system while ensuring stable operation. Furthermore, it can be seen from Fig 8(c) that the frequency drop rate is the smallest under CM3, indicating that the DC side effectively provides inertial support for the system effectively. It can be seen from Fig. 8(d), (8e), and (f) that the $\Delta f_1 - \Delta f_3$ are 0.03, 0.04 and 0.18 Hz, $\Delta P_1 - \Delta P_3$ are 2.84, 3.31 and 5.87 MW. By adaptively adjusting the droop coefficient, VSC2, which has a larger power margin, bear more unbalanced power and enhances the operational stability of the system.

4.3. Sudden increase of power grid load at the sending end system

At t = 5 s, AC2 load decreases by 20 MW, the simulation results are shown in Fig. 9.

As can be seen in Fig. 9(b), under conventional droop control, Δf_2 is 0.26 Hz and both Δf_1 and Δf_3 are 0, the VSC-station does not provide power support to the faulty system. When CM2 control is used, Δf_2 decreases to 0.19 Hz, Δf_1 and Δf_3 are 0.016 Hz and 0.045 Hz, respectively, and $\Delta P_1 - \Delta P_3$ are 1.73, 5.48 and 3.5 MW, respectively. After the VSC-MTDC system reaches a new steady state, the frequency drop of the faulty AC system is significantly reduced, which improves the operational stability of the system.

Under the control strategy of this paper, the droop coefficient is dynamically adjusted according to the real-time power margin of the VSC-station to improve the unbalanced power ration, and

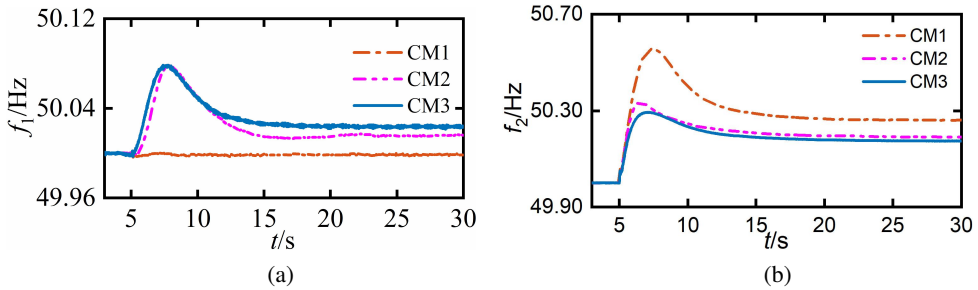

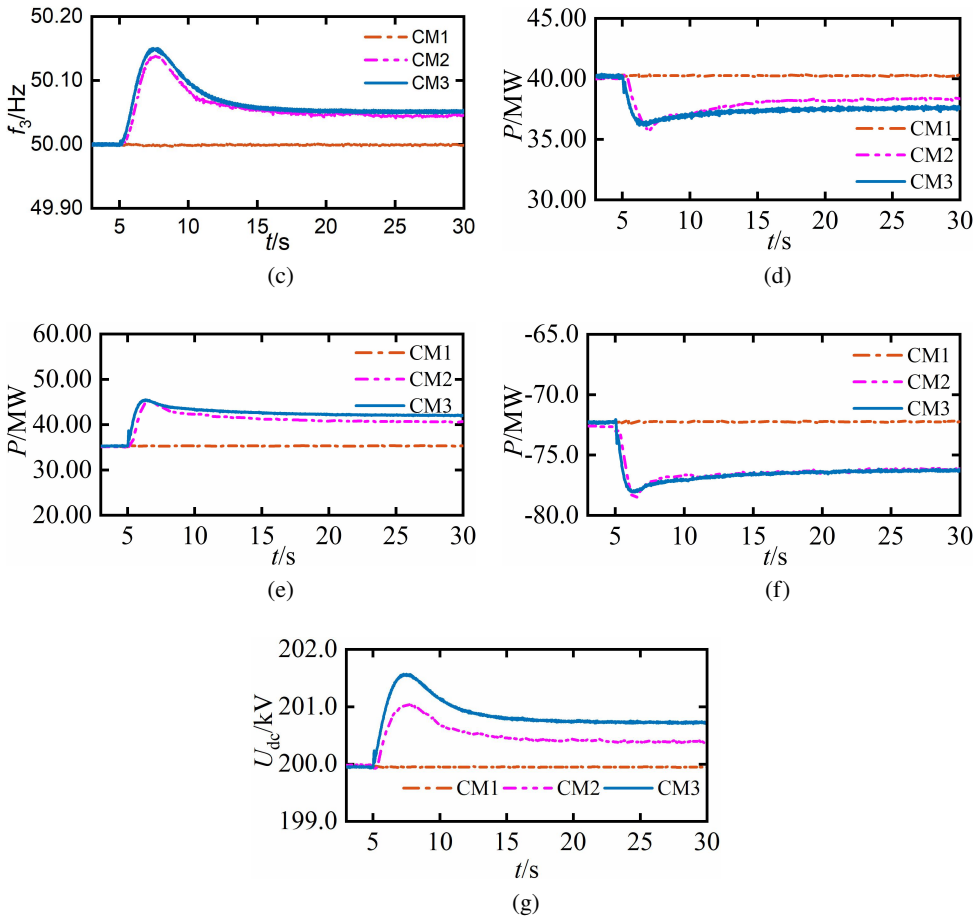

Fig. 9. AC2 active load decrease simulation: AC1 frequency (a); AC2 frequency (b); AC3 frequency (c); VSC1 active power (d); VSC2 active power (e); VSC3 active power (*f*); system DC voltage (g)

Δf_2 decreases to 0.17 Hz. It can be seen from Fig. 9(d), (9e), and (*f*) that the Δf_1 and Δf_2 are 0.02 and 0.05 Hz, $\Delta P_1 - \Delta P_3$ are 2.61, 6.68 and 4.03 MW. As the power support capability of the AC system is further enhanced, the DC voltage deviation is relatively large.

4.4. Single-phase short circuit fault of AC1 system

At $t = 5$ s, a single-phase short circuit fault occurs in AC1, which lasts for 0.05 s. The simulation results are shown in Fig. 10.

From Fig. 10(a), it can be seen that the maximum frequency deviations under the three control strategies are 0.61, 0.55 and 0.49 Hz in the case of a single-phase short-circuit fault in AC1. The control strategy in this paper can reduce the frequency deviation under transient faults to a certain extent and can quickly enter the frequency recovery phase.

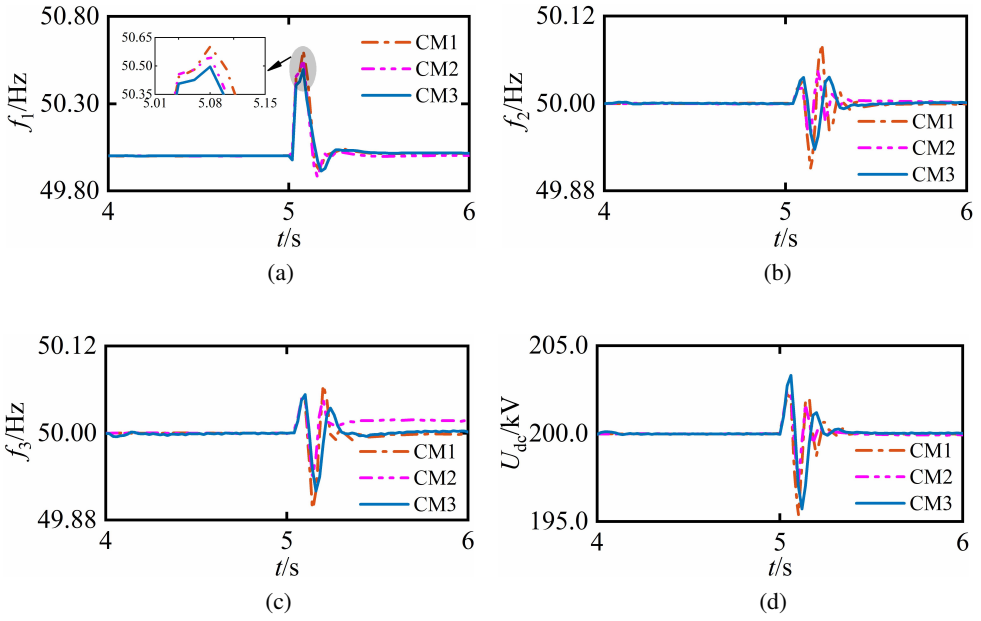

Fig. 10. AC1 single-phase short circuit simulation: AC1 frequency (a); AC2 frequency (b); AC3 frequency (c); system DC voltage (d)

5. Conclusion

In this paper, a virtual synchronous machine control strategy based on a virtual governor is proposed for an interconnected VSC-MTDC system consisting of multiple AC grids. The strategy is based on the droop control of the VSC-MTDC system, which allows it to simulate the inertia response and primary frequency regulation capability of synchronous generators, and the following conclusions are obtained.

1. By coupling the DC-side active power and the AC-side system frequency through virtual inertia technology, the VSC-MTDC system can be made to provide a primary frequency modulation function and inertia response capability.
2. By introducing the converter station power margin into the droop coefficient, the power distribution within the DC system can be automatically adjusted to reduce the DC voltage deviation.
3. The power support capability of the interconnected AC system can be used to effectively reduce the frequency deviation of the accident end system and achieve inter-regional resource complementarity.

Based on the work in this paper, control strategies for joint frequency regulation of wind power and VSC-MTDC systems can be investigated in the future to further reduce the frequency deviation of the accident end system.

Acknowledgements

This research was funded by the Key Projects of Colleges and Universities in Henan Province, grant number 23A470011; the Major Science and Technology Projects in Henan Province, grant number 221100240500.

References

[1] Su M.H., Li Y.K., Dong H.Y., Liu K.Q., Zou W.W., *Subsynchronous oscillation and its mitigation of VSC-MTDC with doubly-fed induction generator-based wind farm integration*, Archives of Electrical Engineering, vol. 70, no. 1, pp. 53–72 (2021), DOI: 10.24425/aee.2021.136052.

[2] Rian F.M., Robin P., *Assessing the impact of VSC-HVDC on the interdependence of power system dynamic performance in uncertain mixed AC/DC systems*, IEEE Transactions on Power Systems, vol. 35, no. 1, pp. 63–74 (2019), DOI: 10.1109/TPWRS.2019.2914318.

[3] Ngo M.K., Nguyen A.T., Doan D.T., *Experimental study on fault ride-through capability of VSC-based HVDC transmission system*, Archives of Electrical Engineering, vol. 70, no. 1, pp. 37–51 (2021), DOI: 10.24425/aee.2021.136051.

[4] Zhang J.Y., Li M.J., *Analysis of the frequency characteristic of the power systems highly penetrated by new energy generation*, Proceedings of the CSEE, vol. 40, no. 11, pp. 3498–3507 (2020), DOI: 10.13334/j.0258-8013.pcsee.191265.

[5] Liu Y.C., Tim C.G., Kumars R., Ali R., Xu D.G., *A new droop coefficient design method for accurate power-sharing in VSC-MTDC systems*, IEEE Access, vol. 7, pp. 47605–47614 (2029), DOI: 10.1109/ACCESS.2019.2909044.

[6] Li B., Li Q.Q., Wang Y.Z., Wen W.J., Li B.T., Xu L., *A novel method to determine droop coefficients of DC voltage control for VSC-MTDC system*, IEEE Transactions on Power Delivery, vol. 35, no. 5, pp. 2196–2211 (2020), DOI: 10.1109/TPWRD.2019.2963447.

[7] Li J.Y., Dong H.Y., *Distributed collaborative optimization DC voltage control strategy for VSC–MTDC system with renewable energy integration*, Archives of Electrical Engineering, vol. 71, no. 2, pp. 325–342 (2022), DOI: 10.24425/aee.2022.140714.

[8] Zhu J.B., Wang X.N., Zhao J.B., Yu L.J., Li S.X., Li Y.W., Josep M.G., Wang C.S., *Inertia emulation and fast frequency-droop control strategy of a point-to-point VSC-HVDC transmission system for asynchronous grid interconnection*, IEEE Transactions on Power Electronics, vol. 37, pp. 6530–6543 (2022), DOI: 10.1109/TPEL.2021.3139960.

[9] Gao B.T., Xia C.P., Zhang L., Chen N., *Modeling and parameters design for rectifier side of VSC-HVDC based on virtual synchronous machine technology*, Proceedings of the CSEE, vol. 37, no. 2, pp. 534–543 (2017), DOI: 10.13334/j.0258-8013.pcsee.161644.

[10] Wang W.Y., Li Y., Cao Y.J., Ulf H., Christian R., *Adaptive droop control of VSC-MTDC system for frequency support and power sharing*, IEEE Transactions on Power Systems, vol. 33, no. 2, pp. 1264–1274 (2018), DOI: 10.1109/TPWRS.2017.2719002.

[11] Fernando D.B., Jose L.D.G., *Coordinated frequency control using MT-HVDC grids with wind power plants*, IEEE Transactions on Sustainable Energy, vol. 7, no. 7, pp. 213–220 (2016), DOI: 10.1109/TSTE.2015.2488098.

[12] Miao Z.X., Fan L.L., Dale O., Sunnaraya Y., *Wind farms with HVDC delivery in inertial response and primary frequency control*, IEEE Transactions on Energy Conversion, vol. 25, no. 4, pp. 1171–1178 (2010), DOI: 10.1109/TEC.2010.2060202.

[13] Li C., Li Y., Cao Y.J., Zhu H.Q., Christian R., Ulf H., *Virtual synchronous generator control for damping DC-side resonance of VSC-MTDC system*, IEEE Journal of Emerging and Selected Topics in Power Electronics, vol. 6, no. 3, pp. 1054–1064 (2018), DOI: 10.1109/JESTPE.2018.2827361.

[14] Wang W.Y., Jiang L., Cao Y.J., Li Y., *A parameter alternating VSG controller of VSC-MTDC systems for low frequency oscillation damping*, IEEE Transactions on Power Systems, vol. 35, no. 6, pp. 4609–4621 (2020), DOI: 10.1109/TPWRS.2020.2997859.

[15] Zhong Q.C., *Virtual synchronous machines and autonomous power systems*, Proceedings of the CSEE, vol. 37, no. 2, pp. 336–349 (2017), DOI: 10.13334/j.0258-8013.pcsee.162325.

[16] Luo L., Wang Y.H., Chen S.Y., Wan L.B., *Adaptive droop control of muti-terminal direct current based on virtual synchronous generator control strategy*, Science Technology and Engineering, vol. 21, no. 17, pp. 7116–7121 (2021), DOI: 10.3969/j.issn.1671-1815.2021.17.021.

[17] Cao Y.J., Wang W.Y., Li Y., Tan Y., Chen C., He L., Hager U., Christian R., *A virtual synchronous generator control strategy for VSC-MTDC systems*, IEEE Transactions on Energy Conversion, vol. 33, no. 2, pp. 750–761 (2018), DOI: 10.1109/TEC.2017.2780920.

[18] Liu Z.Y., Wang W.Q., Wang H.Y., Yuan C.Y., Wang L., Li Y.Q., Ding W.B., *VSC-HVDC inverter control strategy based on VSG technology*, Electric Power Construction, vol. 40, no. 2, pp. 100–108 (2019), DOI: 10. 3969 /j. issn. 1000-7229. 2019. 02. 013.

[19] Zhang Y.X., Cheng Y.C., Liu K.X., Han Y., *Influence of control parameters on synchronization stability of virtual synchronous generator*, Archives of Electrical Engineering, vol. 71, no. 4, pp. 811–828 (2022), DOI: 10.24425/aee.2022.142110.

[20] Cui J.T., Li Z., He P., Gong Z.J., Dong J., *Electromechanical transient modeling of energy storage based on virtual synchronous machine technology*, Archives of Electrical Engineering, vol. 71, no. 3, pp. 581–599 (2022), DOI: 10.24425/aee.2022.141672.

[21] Zhu J.B., Campbell D.B., Grain P.A., Andrew J.R., Chris G.B., *Inertia emulation control strategy for VSC-HVDC transmission systems*, IEEE Transactions on Power Systems, vol. 28, no. 2, pp. 1277–1287 (2013), DOI: 10.1109/TPWRS.2012.2213101.

[22] Shen Z.P., Zhu J.B., Ge L.J., Bu S.Q., Zhao J.B., Chung C.Y., Li X.L., Wang C.S., *Variable-inertia emulation control scheme for VSC-HVDC transmission systems*, IEEE Transactions on Power Systems, vol. 37, no. 1, pp. 629–639 (2022), DOI: 10.1109/TPWRS.2021.3088259.

[23] Li C.S., Li Y.K., Guo J., He P., *Research on emergency DC power support coordinated control for hybrid multi-infeed HVDC system*, Archives of Electrical Engineering, vol. 69, no. 1, pp. 5–21 (2020), DOI: 10.24425/aee.2022.140714.

[24] Liu Z.X., Qin L., Yang S.Q., Zhou Z.Y., Wang Q., Zheng J.W., Liu K.P., *Review on virtual synchronous generator control technology of power electronic converter in power system based on new energy*, Power System Technology, vol. 47, no. 1, pp. 1–16 (2023), DOI: 10.13335/j.1000-3673.pst.2022.0083.

[25] Huang Z.D., *Adaptive integrated coordinated control strategy for MMC-MTDC Systems*, 2018 International Conference on Power System Technology, pp. 2440–2447 (2018), DOI: 10.1109/POWERCON.2018.8601697.

[26] Peng Q., Liu T.Q., Zhang Y.M., Li B.H., Tang S.Y., *Adaptive droop control of VSC based DC grid considering power margin and system stability*, Proceedings of the CSEE, vol. 38, no. 12, pp. 3498–3506 (2018), DOI: 10.13334/j.0258-8013.pcsee.171464.

[27] Liu H.Y., Liu C.R., Jiang S.W., *Dynamic additional frequency control strategy for multi-terminal flexible DC transmission system*, Electric Power Automation Equipment, vol. 42, no. 1, pp. 164−170 (2022), DOI: 10.16081/j.epae.202109025.